X-Ray Polarization of the Eastern Lobe of SS 433

Philip Kaaret, Riccardo Ferrazzoli, Stefano Silvestri, Michela Negro, Alberto Manfreda, Kinwah Wu, Enrico Costa, Paolo Soffitta, Samar Safi-Harb, Juri Poutanen, et al.

The Astrophysical Journal Letters, 961:L12 (8pp), 2024 January 20 https://doi.org/10.3847/2041-8213/ad103b

X-Ray Polarization of the Eastern Lobe of SS 433

Philip Kaaret[1], Riccardo Ferrazzoli[2], Stefano Silvestri[3], Michela Negro[4], Alberto Manfreda[5], Kinwah Wu[6], Enrico Costa[2], Paolo Soffitta[2], Samar Safi-Harb[7], Juri Poutanen[8], Alexandra Veledina[8,9], Alessandro Di Marco[2], Patrick Slane[10], Stefano Bianchi[11], Adam Ingram[12], Roger W. Romani[13], Nicolò Cibrario[14,15], Brydyn Mac Intyre[7], Romana Mikušincová[11], Ajay Ratheesh[2], James F. Steiner[10], Jiri Svoboda[16], Stefano Tugliani[14,15], Iván Agudo[17], Lucio A. Antonelli[18,19], Matteo Bachetti[20], Luca Baldini[3,21], Wayne H. Baumgartner[1], Ronaldo Bellazzini[3], Stephen D. Bongiorno[1], Raffaella Bonino[14,15], Alessandro Brez[3], Niccolò Bucciantini[22,23,24], Fiamma Capitanio[2], Simone Castellano[3], Elisabetta Cavazzuti[25], Chien-Ting Chen[26], Stefano Ciprini[19,27], Alessandra De Rosa[2], Ettore Del Monte[2], Laura Di Gesu[25], Niccolò Di Lalla[13], Immacolata Donnarumma[25], Victor Doroshenko[28], Michal Dovčiak[16], Steven R. Ehlert[1], Teruaki Enoto[29], Yuri Evangelista[2], Sergio Fabiani[2], Javier A. García[30], Shuichi Gunji[31], Kiyoshi Hayashida[32,52], Jeremy Heyl[33], Wataru Iwakiri[34], Svetlana G. Jorstad[35,36], Vladimir Karas[16], Fabian Kislat[37], Takao Kitaguchi[29], Jeffery J. Kolodziejczak[1], Henric Krawczynski[38], Fabio La Monaca[2], Luca Latronico[14], Ioannis Liodakis[1], Simone Maldera[14], Frédéric Marin[39], Andrea Marinucci[25], Alan P. Marscher[35], Herman L. Marshall[40], Francesco Massaro[14,15], Giorgio Matt[11], Ikuyuki Mitsuishi[41], Tsunefumi Mizuno[42], Fabio Muleri[2], Chi-Yung Ng[43], Stephen L. O'Dell[1], Nicola Omodei[13], Chiara Oppedisano[14], Alessandro Papitto[18], George G. Pavlov[44], Abel L. Peirson[13], Matteo Perri[18,19], Melissa Pesce-Rollins[3], Pierre-Olivier Petrucci[45], Maura Pilia[20], Andrea Possenti[20], Simonetta Puccetti[19], Brian D. Ramsey[1], John Rankin[2], Oliver J. Roberts[26], Carmelo Sgrò[3], Gloria Spandre[3], Douglas A. Swartz[26], Toru Tamagawa[29], Fabrizio Tavecchio[46], Roberto Taverna[47], Yuzuru Tawara[41], Allyn F. Tennant[1], Nicholas E. Thomas[1], Francesco Tombesi[27,48,49], Alessio Trois[20], Sergey S. Tsygankov[8], Roberto Turolla[6,47], Jacco Vink[50], Martin C. Weisskopf[1], Fei Xie[2,51], and Silvia Zane[6]

[1] NASA Marshall Space Flight Center, Huntsville, AL 35812, USA; philip.kaaret@nasa.gov
[2] INAF Istituto di Astrofisica e Planetologia Spaziali, Via del Fosso del Cavaliere 100, I-00133 Roma, Italy
[3] Istituto Nazionale di Fisica Nucleare, Sezione di Pisa, Largo B. Pontecorvo 3, I-56127 Pisa, Italy
[4] Department of Physics and Astronomy, Louisiana State University, Baton Rouge, LA 70803, USA
[5] Istituto Nazionale di Fisica Nucleare, Sezione di Napoli, Strada Comunale Cinthia, I-80126 Napoli, Italy
[6] Mullard Space Science Laboratory, University College London, Holmbury St Mary, Dorking, Surrey RH5 6NT, UK
[7] University of Manitoba, Department of Physics & Astronomy, Winnipeg, MB R3T 2N2, Canada
[8] Department of Physics and Astronomy, 20014 University of Turku, Finland
[9] Nordita, KTH Royal Institute of Technology and Stockholm University, Hannes Alfvéns väg 12, SE-10691 Stockholm, Sweden
[10] Center for Astrophysics, Harvard & Smithsonian, 60 Garden Street, Cambridge, MA 02138, USA
[11] Dipartimento di Matematica e Fisica, Università degli Studi Roma Tre, Via della Vasca Navale 84, I-00146 Roma, Italy
[12] School of Mathematics, Statistics, and Physics, Newcastle University, Newcastle upon Tyne NE1 7RU, UK
[13] Department of Physics and Kavli Institute for Particle Astrophysics and Cosmology, Stanford University, Stanford, CA 94305, USA
[14] Istituto Nazionale di Fisica Nucleare, Sezione di Torino, Via Pietro Giuria 1, I-10125 Torino, Italy
[15] Dipartimento di Fisica, Università degli Studi di Torino, Via Pietro Giuria 1, I-10125 Torino, Italy
[16] Astronomical Institute of the Czech Academy of Sciences, Boční II 1401/1, 14100 Praha 4, Czech Republic
[17] Instituto de Astrofísicade Andalucía—CSIC, Glorieta de la Astronomía s/n, E-18008 Granada, Spain
[18] INAF Osservatorio Astronomico di Roma, Via Frascati 33, I-00040 Monte Porzio Catone (RM), Italy
[19] Space Science Data Center, Agenzia Spaziale Italiana, Via del Politecnico snc, I-00133 Roma, Italy
[20] INAF Osservatorio Astronomico di Cagliari, Via della Scienza 5, I-09047 Selargius (CA), Italy
[21] Dipartimento di Fisica, Università di Pisa, Largo B. Pontecorvo 3, I-56127 Pisa, Italy
[22] INAF Osservatorio Astrofisico di Arcetri, Largo Enrico Fermi 5, I-50125 Firenze, Italy
[23] Dipartimento di Fisica e Astronomia, Università degli Studi di Firenze, Via Sansone 1, I-50019 Sesto Fiorentino (FI), Italy
[24] Istituto Nazionale di Fisica Nucleare, Sezione di Firenze, Via Sansone 1, I-50019 Sesto Fiorentino (FI), Italy
[25] Agenzia Spaziale Italiana, Via del Politecnico snc, I-00133 Roma, Italy
[26] Science and Technology Institute, Universities Space Research Association, Huntsville, AL 35805, USA
[27] Istituto Nazionale di Fisica Nucleare, Sezione di Roma "Tor Vergata," Via della Ricerca Scientifica 1, I-00133 Roma, Italy
[28] Institut für Astronomie und Astrophysik, Universität Tübingen, Sand 1, D-72076 Tübingen, Germany
[29] RIKEN Cluster for Pioneering Research, 2-1 Hirosawa, Wako, Saitama 351-0198, Japan
[30] California Institute of Technology, Pasadena, CA 91125, USA
[31] Yamagata University, 1-4-12 Kojirakawa-machi, Yamagata-shi 990-8560, Japan
[32] Osaka University, 1-1 Yamadaoka, Suita, Osaka 565-0871, Japan
[33] University of British Columbia, Vancouver, BC V6T 1Z4, Canada
[34] International Center for Hadron Astrophysics, Chiba University, Chiba 263-8522, Japan
[35] Institute for Astrophysical Research, Boston University, 725 Commonwealth Avenue, Boston, MA 02215, USA
[36] Department of Astrophysics, St. Petersburg State University, Universitetsky pr. 28, Petrodvoretz, 198504 St. Petersburg, Russia
[37] Department of Physics and Astronomy and Space Science Center, University of New Hampshire, Durham, NH 03824, USA
[38] Physics Department and McDonnell Center for the Space Sciences, Washington University in St. Louis, St. Louis, MO 63130, USA
[39] Université de Strasbourg, CNRS, Observatoire Astronomique de Strasbourg, UMR 7550, F-67000 Strasbourg, France
[40] MIT Kavli Institute for Astrophysics and Space Research, Massachusetts Institute of Technology, 77 Massachusetts Avenue, Cambridge, MA 02139, USA
[41] Graduate School of Science, Division of Particle and Astrophysical Science, Nagoya University, Furo-cho, Chikusa-ku, Nagoya, Aichi 464-8602, Japan
[42] Hiroshima Astrophysical Science Center, Hiroshima University, 1-3-1 Kagamiyama, Higashi-Hiroshima, Hiroshima 739-8526, Japan
[43] Department of Physics, University of Hong Kong, Pokfulam, Hong Kong
[44] Department of Astronomy and Astrophysics, Pennsylvania State University, University Park, PA 16801, USA
[45] Université Grenoble Alpes, CNRS, IPAG, F-38000 Grenoble, France
[46] INAF Osservatorio Astronomico di Brera, via E. Bianchi 46, I-23807 Merate (LC), Italy

[47] Dipartimento di Fisica e Astronomia, Università degli Studi di Padova, Via Marzolo 8, I-35131 Padova, Italy
[48] Dipartimento di Fisica, Università degli Studi di Roma "Tor Vergata," Via della Ricerca Scientifica 1, I-00133 Roma, Italy
[49] Department of Astronomy, University of Maryland, College Park, MD 20742, USA
[50] Anton Pannekoek Institute for Astronomy & GRAPPA, University of Amsterdam, Science Park 904, 1098 XH Amsterdam, The Netherlands
[51] Guangxi Key Laboratory for Relativistic Astrophysics, School of Physical Science and Technology, Guangxi University, Nanning 530004, People's Republic of China
Received 2023 September 19; revised 2023 November 7; accepted 2023 November 27; published 2024 January 16

Abstract

How astrophysical systems translate the kinetic energy of bulk motion into the acceleration of particles to very high energies is a pressing question. SS 433 is a microquasar that emits TeV γ-rays indicating the presence of high-energy particles. A region of hard X-ray emission in the eastern lobe of SS 433 was recently identified as an acceleration site. We observed this region with the Imaging X-ray Polarimetry Explorer and measured a polarization degree in the range 38%–77%. The high polarization degree indicates the magnetic field has a well-ordered component if the X-rays are due to synchrotron emission. The polarization angle is in the range $-12°$ to $+10°$ (east of north), which indicates that the magnetic field is parallel to the jet. Magnetic fields parallel to the bulk flow have also been found in supernova remnants and the jets of powerful radio galaxies. This may be caused by interaction of the flow with the ambient medium.

Unified Astronomy Thesaurus concepts: High mass x-ray binary stars (733); Jets (870); High energy astrophysics (739); Supernova remnants (1667); Astrophysical black holes (98)

1. Introduction

A variety of astrophysical systems are capable of translating the kinetic energy of bulk motion into the acceleration of particles to very high energies. Some examples include supernova remnants (Vink 2012), the jets of supermassive black holes (Blandford et al. 2019) and stellar-mass compact objects (Mirabel & Rodríguez 1999), and explosive events such as γ-ray bursts (Kumar & Zhang 2015). Understanding the physical conditions within the acceleration regions is key to deciphering the acceleration process.

SS 433 is a stellar binary system exhibiting jets that generate TeV γ-rays revealing the presence of energetic particles (Margon 1984; Abeysekara et al. 2018). SS 433 contains a stellar-mass compact object (likely a black hole) accreting from a supergiant companion (Fabrika 2004) and lies within the Milky Way at a distance of 5.5 kpc (Hjellming & Johnston 1981; Blundell & Bowler 2004). The compact object launches bipolar jets (with a position angle of 100° and inclined 80° to our line of sight) containing ionized matter moving at a bulk speed of $0.26c$ (Margon 1984). The jets precess with a period of 162.5 days and an opening angle of 20° and interact with the surrounding supernova remnant, W50, creating two lobes east and west from SS 433 and a unique morphology denoted as the "Manatee."[53]

The jet X-ray emission has a thermal spectrum with prominent line emission within 0.16 pc of SS 433 (Marshall et al. 2002; Migliari et al. 2002). The spectrum is nonthermal in the east ("e1") and west ("w1") lobes starting about 30 pc from SS 433 (Yamauchi et al. 1994; Safi-Harb & Ögelman 1997; Safi-Harb & Petre 1999). Soft thermal emission is seen from the termination shock at the jet end (Safi-Harb & Ögelman 1997; Brinkmann et al. 2007). The X-ray spectra of the e1 and w1 lobes are consistent with synchrotron radiation from energetic electrons (Watson et al. 1983; Safi-Harb & Petre 1999). The High Altitude Water Cherenkov (HAWC) observatory, in Mexico, detected very high-energy (VHE) γ-ray emission from the e1 and w1 lobes extending up to at least 25 TeV indicating the presence of particles with energies of hundreds of TeV (Abeysekara et al. 2018). The VHE γ-ray emission has been confirmed with the Large High Altitude Air Shower Observatory (LHAASO; Cao et al. 2023). Detection of γ-ray emission from the lobes with the High Energy Stereoscopic System (H.E.S.S.) has also been reported (Olivera-Nieto 2022). The TeV emission and the nonthermal X-ray emission is localized to the lobes, which suggests that particle acceleration occurs in the jet at significant distances away from SS 433.

Using XMM-Newton and NuSTAR, Safi-Harb et al. (2022) identified a region (the "Head"; see the bottom plot of Figure 1) of nonthermal hard X-ray emission (3–30 keV) at $\sim 18'$ (29 pc) east of SS 433 coincident with the onset of X-ray emission in the e1 lobe closest to SS 433. Assuming the hard X-rays are synchrotron radiation, the hard spectrum (photon index $\Gamma \approx 1.6$) suggests that this is the site of the acceleration of the high-energy particles. This is supported by the morphology of the X-ray emission, which shows the hardest X-ray emission closest to SS 433, with lower-energy X-rays forming a cometary tail pointed away from SS 433. The "Head" does not appear to have counterparts at longer wavelengths; thus, no polarization information is available.

We observed the "Head" region using the Imaging X-ray Polarimetry Explorer (IXPE) in order to measure the polarization of the X-ray emission and constrain the geometry of the magnetic field. We describe the observations and our analysis in Section 2 and present the X-ray polarization results in Section 3. We discuss the results and the implications for the acceleration mechanism in Section 4.

2. Observations and Data Reduction

IXPE is the first satellite mission dedicated to X-ray polarimetry in the 2–8 keV band (Weisskopf et al. 2022). It contains three X-ray telescopes, each consisting of a Mirror Module Assembly (Ramsey et al. 2022) and a polarization-sensitive gas-pixel detector unit (DU; Costa et al. 2001; Baldini et al. 2021; Soffitta et al. 2021), that enable imaging X-ray polarimetry of extended sources. IXPE provides an angular resolution of $\sim 30''$

[52] Deceased.
[53] https://www.nrao.edu/pr/2013/w50/

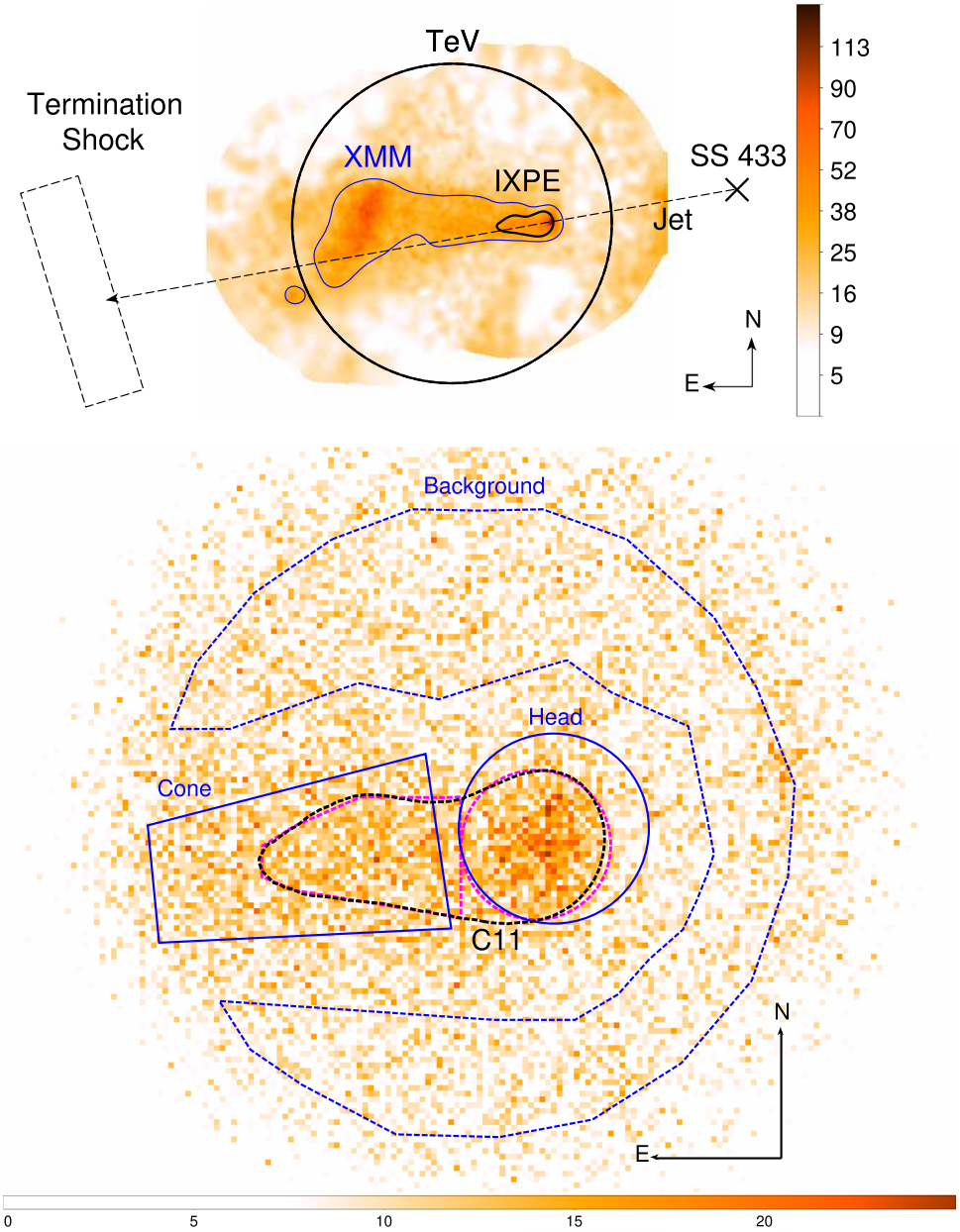

Figure 1. X-ray images of the eastern lobe of SS 433. (Top) Mosaic of XMM-Newton data in the 0.3–10 keV band. The cross marks the location of the binary. The dashed line indicates the jet axis (Hjellming & Johnston 1981), and the dashed rectangle marks the jet termination shock. The blue contour is 25 counts pixel^{-1} in the XMM-Newton image. The black contour is the IXPE source region. The black circle is the HAWC error circle and has a radius of 15′. (Bottom) X-ray image from IXPE in the 2–5 keV band. C11 marks the black contour used as the IXPE source region. The partially overlapping magneta contours indicate the forward region (overlapping the "Head") and trailing region (overlapping the "Cone") used for spatially resolved polarization analysis. The blue dashed contour marks the background region. The blue circle is the "Head" region and the blue quadrilateral is the "Cone" region from Safi-Harb et al. (2022). The black arrows have a length of 2′ (3.2 pc).

(half-power diameter). The overlap of the fields of view of the three DUs is circular with a diameter of 12.′9. The DUs record the tracks of photoelectrons produced by X-rays to enable measurement of linear X-ray polarization.

IXPE observed the eastern lobe of SS 433 from 2023 April 19 to 2023 May 9 with a gap on 2023 May 2 due to observations of another target. The target coordinates (R.A. = 288.°27799, decl. = 4.°93573) were selected to cover the region of hard X-ray emission identified by Safi-Harb et al. (2022). The target is 5.′7 from the LHAASO position and within the error circle.

Because our target is extended and relatively faint, the photon event list was processed to reduce the instrumental background that is induced by Earth albedo and primary energetic particles and secondaries produced in their interactions in the detectors or elsewhere on the spacecraft. The rejection algorithm is described in Di Marco et al. (2023) and removes ∼40% of the background events and a negligible fraction (∼1%) of good events. The main components of the residual background are secondary positrons and a few primary protons that cannot be morphologically distinguished from X-ray initiated photoelectron tracks (Xie et al. 2021). We also removed times of high background found following bright solar flares (likely associated with coronal mass ejections) and surrounding intervals when IXPE crosses the

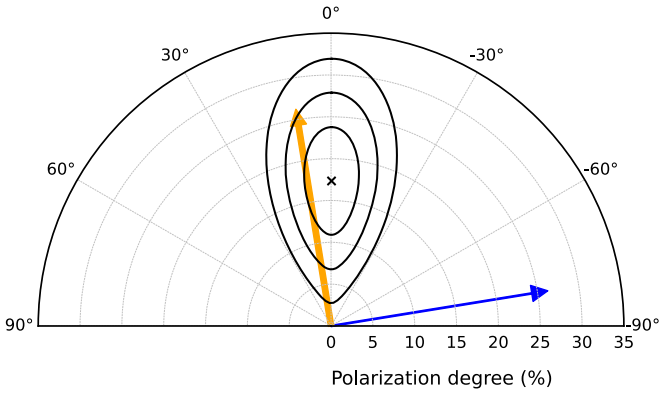

Figure 2. Contour plots of the polarization degree and angle measured with pcube. Position angles are measured positive east of north. The cross marks the measured values. The contours are at the 68.27%, 95.45%, and 99.73% confidence intervals. The blue arrow indicates the direction from the lobe to the compact object, while the orange arrow is perpendicular.

South Atlantic Anomaly. These backgrounds appear as short-term increases in counting rate, and we removed times when the count rate was higher than the mean rate plus 3 times the rms of the rate (Forsblom et al. 2023). The technique has been important for the study of faint sources such as Galactic center clouds and supernova remnants with IXPE (Marin et al. 2023; Zhou et al. 2023). After filtering, the total livetime was 800.7, 791.8, and 789.2 ks for DU1, DU2, and DU3, respectively. The background is higher at the field of view edges of each DU, but relatively uniform across the central 10′ diameter (Di Marco et al. 2023). We limit our analysis to this central region.

We selected an energy band to optimize the signal from the source versus the background, both instrumental and from the cosmic X-ray background. We extracted a source spectrum using the "Head" region defined by Safi-Harb et al. (2022) and a background spectrum from a nearby region without strong diffuse emission. Scaling for the region sizes, the source spectrum is above the background spectrum in the energy band of 2–5 keV, which we use for all subsequent analysis.

The IXPE image in this band is shown in Figure 1 along with an XMM-Newton mosaic in the 0.3–10 keV band (Safi-Harb et al. 2022). We define an IXPE source region, that we refer to as "C11," by drawing a contour corresponding to 11 counts per pixel in the IXPE map using the SAOImage DS9 image display tool with the smoothing parameter set to 16 (Smithsonian Astrophysical Observatory 2000). The region covers most of the "Head" and "Cone" regions. We define a background region (shown as a dashed line in Figure 1) that avoids areas of strong diffuse emission and is within the central region of the image with good polarization response.

We extracted events within the source and background regions using IXPEOBSSIM version 30.5.0 (Baldini et al. 2022). We calculated polarization data cubes in the 2–5 keV energy band using the pcube algorithm in the xpbin tool and spectra of I, Q, and U Stokes parameters with PHA1, PHAQ1, and PHAU1 algorithms in xpbin. We performed spectropolarimetric analysis using XSPEC version 12.13.1. We used version 12 of IXPE instrument response files and performed an unweighted analysis for both pcube and XSPEC.

3. Polarization Results

Figure 2 shows the polarization of the events from the C11 region as measured using the model-independent pcube algorithm. The observed polarization degree (PD) is $17.3\% \pm 4.3\%$ and the electric vector position angle (EVPA) is $-0.^{\circ}2 \pm 7.^{\circ}0$ (all uncertainties are 68% confidence). Position angles are measured counterclockwise from north in the equatorial coordinate system as per the convention of the International Astronomical Union. The probability that the signal is a random fluctuation from an unpolarized source is 2.4×10^{-4}. This is equivalent to a 3.7σ confidence level. We note that the energy band and source region selection were based on the intensity data alone; thus, there is only one trial for calculation of the significance of the polarization detection. The events include the X-ray emission from the lobe of SS 433, the cosmic X-ray background, and the residual instrumental background. All are expected to be unpolarized except for the emission from the lobe. Thus, the result indicates a highly probable detection of polarization in the X-ray emission of the lobe.

Scaling from the background region, we estimate that 30% of the counts are from the lobe and 70% are from instrumental or astrophysical backgrounds. Utilizing the additive nature of the Stokes parameters, we calculated the Stokes I, Q, and U for the source and background regions and then subtracted the background from the source after scaling for the different region areas. After background subtraction, we estimate the PD of the lobe emission as $62\% \pm 15\%$ and the EVPA as $2.^{\circ}8 \pm 7.^{\circ}0$. As expected for unpolarized backgrounds, the EVPA is consistent with the results before background subtraction. The PD is consistent with that calculated using the polarization dilution equation (Equation (2)) in Di Marco et al. (2023).

We also divided the C11 region into two parts, see Figure 1, and performed a background-subtracted polarization analysis. The circular region covering the forward region has $\mathrm{PD} = 59\% \pm 17\%$, $\mathrm{EVPA} = 6^{\circ} \pm 8^{\circ}$, and a chance probability of 0.0044. While the polygon covering the trailing region does not provide a significant detection, yielding a chance probability of 0.033, the PD ($48\% \pm 18\%$) and EVPA ($4^{\circ} \pm 10^{\circ}$) are consistent with those of C11. The lower detection significance of the forward region relative to C11 suggests that the polarization signal is not concentrated in the forward region.

We measured the polarization of the events from the background region and found that it is consistent with zero. The same background region is used for the spectropolarimetic analysis described below. We also investigated three rectangular background regions placed to the north, west, and south of C11 with an area equal to that of C11. The inferred PD and EVPA for the C11 emission are consistent within the statistical uncertainties regardless of the background region used. We also investigated other procedures for the removal of intervals of high background. While the statistical significance of the polarization signal varies, the PD and EVPA after background subtraction remain consistent.

Figure 3 shows the IXPE background-subtracted X-ray spectra for the C11 region. We performed spectropolarimetric analysis using Xspec. This differs from the pcube analysis in that it fully takes into account the response of the instrument including the nondiagonal portion of the energy response. The Stokes I spectra have 80 eV bins below 3 keV and 120 eV above. The Stokes Q

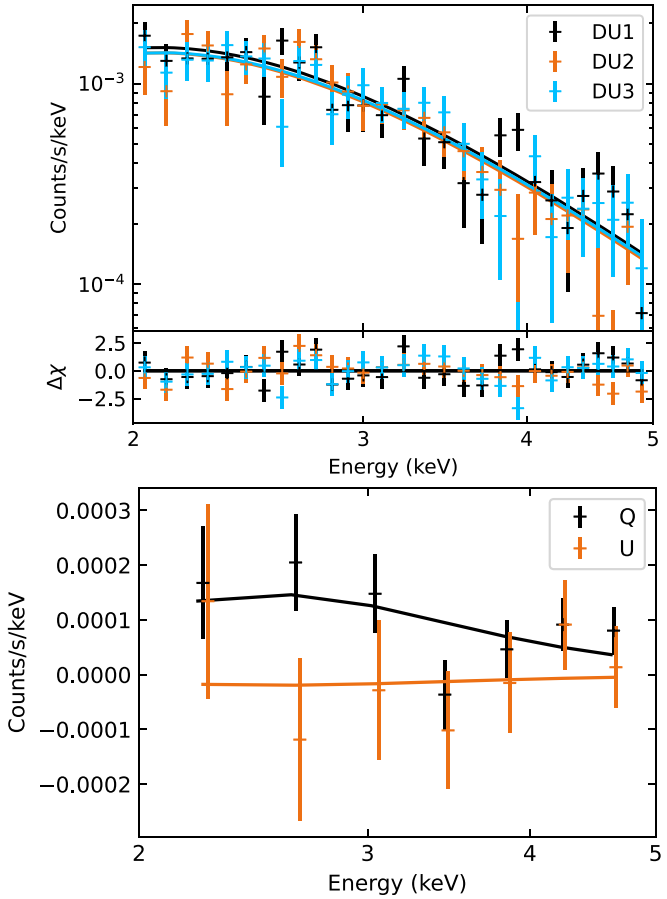

Figure 3. IXPE X-ray spectra of the C11 region. (Top) Intensity (Stokes I) spectra. Data from the three IXPE DUs are shown as crosses: DU1 (black), DU2 (orange), and DU3 (blue). The fitted models, identical except for the normalization, are in the corresponding color. The lower panel shows the fit residuals. (Bottom) Stokes Q (black) and U (orange) spectra. Points are shifted on the x-axis by ±20 eV for clarity. Data from the three DUs are added. The fitted model is shown as a solid line in the same color.

and U spectra have 400 eV bins. We modeled the spectrum using an absorbed power law with constant polarization multiplied by a constant allowed to vary between the three DUs. The column density for the `tbabs` absorption model using the Wilms et al. (2000) abundances was fixed to $1.18 \times 10^{22}\,\mathrm{cm}^{-2}$ as for the "Cone" region in Safi-Harb et al. (2022). The normalization for DU1 was fixed to unity and those for the other DUs were allowed to vary. We find a good spectropolarimetric fit ($\chi^2/\mathrm{dof} = 137.0/123$) with a photon index of $\Gamma = 1.57 \pm 0.14$, consistent with that found by Safi-Harb et al. (2022). The observed flux is 5.8×10^{-13} erg cm^{-2} s^{-1} in the 2–5 keV band. This corresponds to a luminosity of 1.3×10^{34} erg s^{-1} in the 0.3–30 keV band. The EVPA is $-3\overset{\circ}{.}7 \pm 7\overset{\circ}{.}8$, which is consistent with the `pcube` results. The PD is 52% ± 14%, which is consistent with the background-subtracted `pcube` result. The allowed range for PD considering the two analyses is 38% to 77%.

4. Discussion

The high polarization degree found from the C11 region suggests the magnetic field has a well-ordered component, assuming that the X-rays are produced via synchrotron radiation. The maximum polarization for synchrotron radiation is $\Pi = (p+1)/(p+7/3)$ where the electron spectral index is $p = 2\Gamma - 1$. For the C11 region, $\Gamma = 1.57$ and thus $p = 2.14$ and $\Pi = 0.70$. The ratio of the PD after background correction to the maximum polarization is approximately equal to the ratio of the energy in the magnetic field component with uniform direction to that in the total field (Burn 1966). For the C11 region, the lower bound on the PD of 38% indicates at least ≈50% of the field is in the uniform component.

The energy of the electrons producing the emission can be calculated given the magnetic field strength. Assuming equipartition between the energies of the relativistic electrons and the magnetic field, the latter can be estimated from the X-ray luminosity and volume as $B \approx 10\,\mu$G (Safi-Harb et al. 2022). To produce X-rays of energy E_γ, the electron energy needed is $E_e \approx (50\,\mathrm{TeV})(B/10\,\mu\mathrm{G})^{-1/2}(E_\gamma/1\,\mathrm{keV})^{1/2}$. For $E_\gamma = 4$ keV and $B = 10\,\mu$ G, electrons must be accelerated to 100 TeV. The same electrons also produce γ-rays near 25 TeV via inverse-Compton scattering on cosmic microwave background photons. Thus, IXPE probes the magnetic field configuration in the same region producing the VHE emission. The gyroradius for 100 TeV electrons in a 10 μG magnetic field is 0.011 pc, which is much smaller than the transverse diameter of the C11 region of 3 pc. The synchrotron lifetime is 1200 yr (Reynolds 1998). Thus, either the magnetic field is significantly higher than the equipartition estimate or some other loss mechanism dominates over the length of the region.

For synchrotron radiation, the EVPA is perpendicular to the magnetic field. Thus, the magnetic field lies along the direction of the main bulk motion of the jet. The key result of the IXPE observations is that the magnetic field near the acceleration region contains a significant component that is well ordered and parallel to the flow direction. This result places constraints on models of the acceleration process and raises questions on the origin of the magnetic field.

The magnetic field could be intrinsic to the jet. However, while radio polarization measurements show the magnetic field is aligned with the ridge line of the precessing jet near SS 433 (Stirling et al. 2004), at larger distances, the field is instead parallel to the motion of individual knots (Miller-Jones et al. 2008). Thus, the field appears to be determined by the interaction between the individual knots and the ambient medium (Blundell et al. 2018).

The powerful jets in Fanaroff–Riley Class II (FR II) radio galaxies have magnetic fields that are predominantly parallel to the jet axis all across the jet (Bridle & Perley 1984; Asseo & Sol 1987). The radio PDs are high, typically 20%–40% and reaching 50%, e.g., in a knot in the jet of 4C 32.69 that may be analogous to the knot considered here (Potash & Wardle 1980). Velocity shear due to the interaction of the jet with the ambient medium is a natural means to produce a magnetic field aligned with the direction of bulk motion (Blandford 1983).

Young, shell-type supernova remnants show radio EVPAs perpendicular to the flow near the shocks in the outer rims. Recent IXPE observations show similar EVPAs, typically with higher PDs, in the X-ray band (Vink et al. 2022; Ferrazzoli et al. 2023; Zhou et al. 2023). These results indicate magnetic fields parallel to the flow, as seen here. Giacalone & Jokipii (2007) and Inoue et al. (2013) suggest that the magnetic field may stretch as the shock propagates around density fluctuations in the interstellar medium. This stretching can both amplify and align the field with the flow. Again, velocity shear is key to aligning the magnetic field with the flow. Alternatively, West et al. (2017) suggest that the overall field is disordered and that the mean EVPA represents the magnetic field only in localized

regions where electrons are most efficiently accelerated because the magnetic field is parallel to the flow.

We consider several scenarios for acceleration and subsequent propagation and radiation of the energetic particles in the eastern lobe of SS 433. We note that the jet speed of $0.26c$ implies a bulk Lorentz factor of 1.036. The magnetic field of $10\,\mu$G estimated above and a jet density of $0.05\,\mathrm{cm}^{-3}$ (Panferov 2017) implies an Alfvén Mach number of $\sim$900 and a magnetization of $\sigma \sim 2 \times 10^{-4}$. Thus, the interaction is nonrelativistic with a very high Mach number and the jet is hydrodynamical.

One possible scenario is stochastic acceleration in a shock (see, e.g., Caprioli & Spitkovsky 2014; Park et al. 2015) at the leading edge of the e1 lobe followed by synchrotron emission from gradually cooling electrons flowing eastward (Sudoh et al. 2020). In this scenario, acceleration would be localized; Safi-Harb et al. (2022) show a compact region at the leading edge that is bright in the 10–20 keV band and could be the acceleration region. Ordering of the parallel magnetic field would occur downstream of the turbulent shock region. The energetic electrons would suffer radiative loss while propagating downstream from the shock. Thus, the photon index of the nonthermal X-ray emission should gradually steepen eastward as is observed.

A second scenario is stochastic acceleration by turbulence (Petrosian 2012) in the shear interfaces between the jet and ambient medium. Such models have been proposed for FR II radio galaxies and predict hard particle spectra consistent with those observed (Stawarz & Ostrowski 2002; Rieger & Duffy 2004). The acceleration is stochastic; hence, the electron energy spectrum would be a power law with an index similar to that observed. Acceleration is not localized and can occur along the extent of the lobe where there is strong shear; thus, steepening of the spectrum would not be expected over that region. The polarized emission would be predominantly from particles diffused out from the turbulent acceleration shear layer into the interior region with parallel magnetic field (Tavecchio 2021).

A third scenario is acceleration through plasma processes (see, e.g., Melrose 1990) associated with magnetic field reconnection. This may occur at magnetic loops produced by shear (Romanova & Lovelace 1992; Sironi et al. 2021) or at quasi-separatrix layers of adjacent magnetic flux ropes (see Aulanier et al. 2006). The overall field reconfiguration process should be continual and gradual to maintain a quasi-equilibrium between particle acceleration, escape, and radiative loss in order to produce a power-law spectrum with a relatively stable spectral index. While acceleration can occur wherever there is strong shear, the electron spectral index may vary due to local variations in the intensity of reconnection.

We note that Thomson scattering of radiation from the binary system, as an alternative to synchrotron emission, would naturally produce highly polarized X-rays with an EVPA perpendicular to the jet axis. Such a scenario requires an X-ray bright central source and SS 433 may be an ultraluminous X-ray source with the X-ray beam along the jet axis. Waisberg et al. (2019) place an upper bound on the X-ray luminosity of $\lesssim 5 \times 10^{36}\,\mathrm{erg\,s}^{-1}$ in a beam with a 1° opening angle assuming the X-ray spectrum of a hard ultraluminous source (Kaaret et al. 2017). C11 viewed from SS 433 has an opening angle of 3°.2, so the illuminating beam would have a luminosity of $\lesssim 5 \times 10^{37}\,\mathrm{erg\,s}^{-1}$. An optical depth of 3×10^{-4} within C11 would be required to produce the observed luminosity, which is much larger than the expected optical depth of 3×10^{-7} given the density estimate of Panferov (2017). We note that the differing morphology in different energy bands seen with NuSTAR (Safi-Harb et al. 2022) may also present issues with the scattering interpretation.

It may be possible to distinguish between these various models with future IXPE and other X-ray and multiwavelength observations. Deeper observations of the e1 lobe could enable spatially resolved polarization measurements, while observations of the e2 lobe could provide information on downstream evolution of the magnetic field. IXPE observation of the w1 lobe would be of great interest to determine if it also shows an EVPA perpendicular to the jet.

Acknowledgments

The Imaging X-ray Polarimetry Explorer (IXPE) is a joint US and Italian mission. The US contribution is supported by the National Aeronautics and Space Administration (NASA) and led and managed by its Marshall Space Flight Center (MSFC), with industry partner Ball Aerospace (contract NNM15AA18C). The Italian contribution is supported by the Italian Space Agency (Agenzia Spaziale Italiana, ASI) through contract ASI-OHBI-2017-12-I.0, agreements ASI-INAF-2017-12-H0 and ASI-INFN-2017.13-H0, and its Space Science Data Center (SSDC), and by the Istituto Nazionale di Astrofisica (INAF) and the Istituto Nazionale di Fisica Nucleare (INFN) in Italy. A.V. acknowledges support from the Academy of Finland grant 355672.

Facilities: IXPE, XMM-Newton, NuSTAR.

Software: IXPEOBSSIM (Baldini et al. 2022), XSPEC (Arnaud 1996), DS9 (Smithsonian Astrophysical Observatory 2000), ASTROPY (Astropy Collaboration et al. 2013).

ORCID iDs

Philip Kaaret https://orcid.org/0000-0002-3638-0637
Riccardo Ferrazzoli https://orcid.org/0000-0003-1074-8605
Stefano Silvestri https://orcid.org/0000-0002-8665-0105
Michela Negro https://orcid.org/0000-0002-6548-5622
Alberto Manfreda https://orcid.org/0000-0002-0998-4953
Kinwah Wu https://orcid.org/0000-0002-7568-8765
Enrico Costa https://orcid.org/0000-0003-4925-8523
Paolo Soffitta https://orcid.org/0000-0002-7781-4104
Samar Safi-Harb https://orcid.org/0000-0001-6189-7665
Juri Poutanen https://orcid.org/0000-0002-0983-0049
Alexandra Veledina https://orcid.org/0000-0002-5767-7253
Alessandro Di Marco https://orcid.org/0000-0003-0331-3259
Patrick Slane https://orcid.org/0000-0002-6986-6756
Stefano Bianchi https://orcid.org/0000-0002-4622-4240
Adam Ingram https://orcid.org/0000-0002-5311-9078
Roger W. Romani https://orcid.org/0000-0001-6711-3286
Nicolò Cibrario https://orcid.org/0000-0003-3842-4493
Romana Mikušincová https://orcid.org/0000-0001-7374-843X
Ajay Ratheesh https://orcid.org/0000-0003-0411-4243
James F. Steiner https://orcid.org/0000-0002-5872-6061
Jiri Svoboda https://orcid.org/0000-0003-2931-0742
Stefano Tugliani https://orcid.org/0000-0002-3318-9036
Iván Agudo https://orcid.org/0000-0002-3777-6182

Lucio A. Antonelli https://orcid.org/0000-0002-5037-9034
Matteo Bachetti https://orcid.org/0000-0002-4576-9337
Luca Baldini https://orcid.org/0000-0002-9785-7726
Wayne H. Baumgartner https://orcid.org/0000-0002-5106-0463
Ronaldo Bellazzini https://orcid.org/0000-0002-2469-7063
Stephen D. Bongiorno https://orcid.org/0000-0002-0901-2097
Raffaella Bonino https://orcid.org/0000-0002-4264-1215
Alessandro Brez https://orcid.org/0000-0002-9460-1821
Niccolò Bucciantini https://orcid.org/0000-0002-8848-1392
Fiamma Capitanio https://orcid.org/0000-0002-6384-3027
Simone Castellano https://orcid.org/0000-0003-1111-4292
Elisabetta Cavazzuti https://orcid.org/0000-0001-7150-9638
Chien-Ting Chen https://orcid.org/0000-0002-4945-5079
Stefano Ciprini https://orcid.org/0000-0002-0712-2479
Alessandra De Rosa https://orcid.org/0000-0001-5668-6863
Ettore Del Monte https://orcid.org/0000-0002-3013-6334
Laura Di Gesu https://orcid.org/0000-0002-5614-5028
Niccolò Di Lalla https://orcid.org/0000-0002-7574-1298
Immacolata Donnarumma https://orcid.org/0000-0002-4700-4549
Victor Doroshenko https://orcid.org/0000-0001-8162-1105
Michal Dovčiak https://orcid.org/0000-0003-0079-1239
Steven R. Ehlert https://orcid.org/0000-0003-4420-2838
Teruaki Enoto https://orcid.org/0000-0003-1244-3100
Yuri Evangelista https://orcid.org/0000-0001-6096-6710
Sergio Fabiani https://orcid.org/0000-0003-1533-0283
Javier A. García https://orcid.org/0000-0003-3828-2448
Shuichi Gunji https://orcid.org/0000-0002-5881-2445
Jeremy Heyl https://orcid.org/0000-0001-9739-367X
Wataru Iwakiri https://orcid.org/0000-0002-0207-9010
Svetlana G. Jorstad https://orcid.org/0000-0001-6158-1708
Vladimir Karas https://orcid.org/0000-0002-5760-0459
Fabian Kislat https://orcid.org/0000-0001-7477-0380
Jeffery J. Kolodziejczak https://orcid.org/0000-0002-0110-6136
Henric Krawczynski https://orcid.org/0000-0002-1084-6507
Fabio La Monaca https://orcid.org/0000-0001-8916-4156
Luca Latronico https://orcid.org/0000-0002-0984-1856
Ioannis Liodakis https://orcid.org/0000-0001-9200-4006
Simone Maldera https://orcid.org/0000-0002-0698-4421
Frédéric Marin https://orcid.org/0000-0003-4952-0835
Andrea Marinucci https://orcid.org/0000-0002-2055-4946
Alan P. Marscher https://orcid.org/0000-0001-7396-3332
Herman L. Marshall https://orcid.org/0000-0002-6492-1293
Francesco Massaro https://orcid.org/0000-0002-1704-9850
Giorgio Matt https://orcid.org/0000-0002-2152-0916
Tsunefumi Mizuno https://orcid.org/0000-0001-7263-0296
Fabio Muleri https://orcid.org/0000-0003-3331-3794
Chi-Yung Ng https://orcid.org/0000-0002-5847-2612
Stephen L. O'Dell https://orcid.org/0000-0002-1868-8056
Nicola Omodei https://orcid.org/0000-0002-5448-7577
Chiara Oppedisano https://orcid.org/0000-0001-6194-4601
Alessandro Papitto https://orcid.org/0000-0001-6289-7413
George G. Pavlov https://orcid.org/0000-0002-7481-5259
Abel L. Peirson https://orcid.org/0000-0001-6292-1911
Matteo Perri https://orcid.org/0000-0003-3613-4409
Melissa Pesce-Rollins https://orcid.org/0000-0003-1790-8018
Pierre-Olivier Petrucci https://orcid.org/0000-0001-6061-3480
Maura Pilia https://orcid.org/0000-0001-7397-8091
Andrea Possenti https://orcid.org/0000-0001-5902-3731
Simonetta Puccetti https://orcid.org/0000-0002-2734-7835
Brian D. Ramsey https://orcid.org/0000-0003-1548-1524
John Rankin https://orcid.org/0000-0002-9774-0560
Oliver J. Roberts https://orcid.org/0000-0002-7150-9061
Carmelo Sgrò https://orcid.org/0000-0001-5676-6214
Gloria Spandre https://orcid.org/0000-0003-0802-3453
Douglas A. Swartz https://orcid.org/0000-0002-2954-4461
Toru Tamagawa https://orcid.org/0000-0002-8801-6263
Fabrizio Tavecchio https://orcid.org/0000-0003-0256-0995
Roberto Taverna https://orcid.org/0000-0002-1768-618X
Allyn F. Tennant https://orcid.org/0000-0002-9443-6774
Nicholas E. Thomas https://orcid.org/0000-0003-0411-4606
Francesco Tombesi https://orcid.org/0000-0002-6562-8654
Alessio Trois https://orcid.org/0000-0002-3180-6002
Sergey S. Tsygankov https://orcid.org/0000-0002-9679-0793
Roberto Turolla https://orcid.org/0000-0003-3977-8760
Jacco Vink https://orcid.org/0000-0002-4708-4219
Martin C. Weisskopf https://orcid.org/0000-0002-5270-4240
Fei Xie https://orcid.org/0000-0002-0105-5826
Silvia Zane https://orcid.org/0000-0001-5326-880X

References

Abeysekara, A. U., Albert, A., Alfaro, R., et al. 2018, Natur, 562, 82
Arnaud, K. A. 1996, in ASP Conf. Ser. 101, Astronomical Data Analysis Software and Systems V, ed. G. H. Jacoby & J. Barnes (San Francisco, CA: ASP), 17
Asseo, E., & Sol, H. 1987, PhR, 148, 307
Astropy Collaboration, Robitaille, T. P., Tollerud, E. J., et al. 2013, A&A, 558, A33
Aulanier, G., Pariat, E., Démoulin, P., & Devore, C. R. 2006, SoPh, 238, 347
Baldini, L., Barbanera, M., Bellazzini, R., et al. 2021, APh, 133, 102628
Baldini, L., Bucciantini, N., Lalla, N. D., et al. 2022, SoftX, 19, 101194
Blandford, R., Meier, D., & Readhead, A. 2019, ARA&A, 57, 467
Blandford, R. D. 1983, AJ, 88, 245
Blundell, K. M., & Bowler, M. G. 2004, ApJL, 616, L159
Blundell, K. M., Laing, R., Lee, S., & Richards, A. 2018, ApJL, 867, L25
Bridle, A. H., & Perley, R. A. 1984, ARA&A, 22, 319
Brinkmann, W., Pratt, G. W., Rohr, S., Kawai, N., & Burwitz, V. 2007, A&A, 463, 611
Burn, B. J. 1966, MNRAS, 133, 67
Cao, Z., Aharonian, F., An, Q., et al. 2023, arXiv:2305.17030
Caprioli, D., & Spitkovsky, A. 2014, ApJ, 783, 91
Costa, E., Soffitta, P., Bellazzini, R., et al. 2001, Natur, 411, 662
Di Marco, A., Soffitta, P., Costa, E., et al. 2023, AJ, 165, 143
Fabrika, S. 2004, Astrophys. Space Phys. Res., 12, 1
Ferrazzoli, R., Slane, P., Prokhorov, D., et al. 2023, ApJ, 945, 52
Forsblom, S. V., Poutanen, J., Tsygankov, S. S., et al. 2023, ApJL, 947, L20
Giacalone, J., & Jokipii, J. R. 2007, ApJL, 663, L41
Hjellming, R. M., & Johnston, K. J. 1981, ApJL, 246, L141
Inoue, T., Shimoda, J., Ohira, Y., & Yamazaki, R. 2013, ApJL, 772, L20
Kaaret, P., Feng, H., & Roberts, T. P. 2017, ARA&A, 55, 303
Kumar, P., & Zhang, B. 2015, PhR, 561, 1
Margon, B. 1984, ARA&A, 22, 507
Marin, F., Churazov, E., Khabibullin, I., et al. 2023, Natur, 619, 41
Marshall, H. L., Canizares, C. R., & Schulz, N. S. 2002, ApJ, 564, 941
Melrose, D. B. 1990, AuJPh, 43, 703
Migliari, S., Fender, R., & Méndez, M. 2002, Sci, 297, 1673
Miller-Jones, J. C. A., Migliari, S., Fender, R. P., et al. 2008, ApJ, 682, 1141
Mirabel, I. F., & Rodríguez, L. F. 1999, ARA&A, 37, 409

Olivera-Nieto, L. 2022, 7th Heidelberg International Symp. on High-Energy Gamma-Ray Astronomy, https://indico.icc.ub.edu/event/46/contributions/1302/
Panferov, A. A. 2017, A&A, 599, A77
Park, J., Caprioli, D., & Spitkovsky, A. 2015, PhRvL, 114, 085003
Petrosian, V. 2012, SSRv, 173, 535
Potash, R. I., & Wardle, J. F. C. 1980, ApJ, 239, 42
Ramsey, B. D., Bongiorno, S. D., Kolodziejczak, J. J., et al. 2022, JATIS, 8, 024003
Reynolds, S. P. 1998, ApJ, 493, 375
Rieger, F. M., & Duffy, P. 2004, ApJ, 617, 155
Romanova, M. M., & Lovelace, R. V. E. 1992, A&A, 262, 26
Safi-Harb, S., Mac Intyre, B., Zhang, S., et al. 2022, ApJ, 935, 163
Safi-Harb, S., & Ögelman, H. 1997, ApJ, 483, 868
Safi-Harb, S., & Petre, R. 1999, ApJ, 512, 784
Sironi, L., Rowan, M. E., & Narayan, R. 2021, ApJL, 907, L44
Smithsonian Astrophysical Observatory 2000, SAOImage DS9: A utility for displaying astronomical images in the X11 window environment, Astrophysics Source Code Library, ascl:0003.002
Soffitta, P., Baldini, L., Bellazzini, R., et al. 2021, AJ, 162, 208
Stirling, A. M., Spencer, R. E., Cawthorne, T. V., & Paragi, Z. 2004, MNRAS, 354, 1239
Stawarz, Ł., & Ostrowski, M. 2002, ApJ, 578, 763
Sudoh, T., Inoue, Y., & Khangulyan, D. 2020, ApJ, 889, 146
Tavecchio, F. 2021, MNRAS, 501, 6199
Vink, J. 2012, A&ARv, 20, 49
Vink, J., Prokhorov, D., Ferrazzoli, R., et al. 2022, ApJ, 938, 40
Waisberg, I., Dexter, J., Olivier-Petrucci, P., Dubus, G., & Perraut, K. 2019, A&A, 624, A127
Watson, M. G., Willingale, R., Grindlay, J. E., & Seward, F. D. 1983, ApJ, 273, 688
Weisskopf, M. C., Soffitta, P., Baldini, L., et al. 2022, JATIS, 8, 026002
West, J. L., Jaffe, T., Ferrand, G., Safi-Harb, S., & Gaensler, B. M. 2017, ApJL, 849, L22
Wilms, J., Allen, A., & McCray, R. 2000, ApJ, 542, 914
Xie, F., Ferrazzoli, R., Soffitta, P., et al. 2021, APh, 128, 102566
Yamauchi, S., Kawai, N., & Aoki, T. 1994, PASJ, 46, L109
Zhou, P., Prokhorov, D., Ferrazzoli, R., et al. 2023, ApJ, 957, 55